International Journal of Minerals, Metallurgy and Materials
Volume 29, Number 11, November 2022, Page 1981
https://doi.org/10.1007/s12613-021-2353-8

Effect of extrusion on the microstructure and mechanical properties of a low-alloyed Mg–2Zn–0.8Sr–0.2Ca matrix composite reinforced by TiC nano-particles

Zedong Wang[1)], *Kaibo Nie*[1,2),✉], *Kunkun Deng*[1,2)], *and Jungang Han*[1)]

1) College of Materials Science and Engineering, Taiyuan University of Technology, Taiyuan 030024, China
2) Shanxi Key Laboratory of Advanced Magnesium-based Materials, Taiyuan University of Technology, Taiyuan 030024, China
(Received: 4 August 2021; revised: 1 September 2021; accepted: 13 September 2021)

Abstract: A low-alloyed Mg–2Zn–0.8Sr–0.2Ca matrix composite reinforced by TiC nano-particles was successfully prepared by semi-solid stirring under the assistance of ultrasonic, and then the as-cast composite was hot extruded. The results indicated that the volume fraction of dynamical recrystallization and the recrystallized grain size have a certain decline at lower extrusion temperature or rate. The finest grain size of ~0.30 μm is obtained in the sample extruded at 200°C and 0.1 mm/s. The as-extruded sample displays a strong basal texture intensity, and the basal texture intensity increases to 5.937 mud while the extrusion temperature increases from 200 to 240°C. The ultra-high mechanical properties (ultimate tensile strength of 480.2 MPa, yield strength of 462 MPa) are obtained after extrusion at 200°C with a rate of 0.1 mm/s. Among all strengthening mechanisms for the present composite, the grain refinement contributes the most to the increase in strength. A mixture of cleavage facets and dimples were observed in the fracture surfaces of three as-extruded nanocomposites, which explain a mix of brittle-ductile fracture way of the samples.

Keywords: magnesium matrix composite; extrusion; microstructure and mechanical properties; texture; fracture

1. Introduction

Magnesium alloys as the representative of light metal materials, have a broad application prospect in electronics, transportation, and aerospace [1–4]. However, there are still some factors such as low strength, ductility, and poor corrosion [5], which obstruct the widespread applications of magnesium alloys. To enhance the strength and plasticity of magnesium alloys has become the primary issue for broadening the industrial applications of magnesium alloys. Among multitudinous magnesium alloys, the series of Mg–Zn alloys, such as Mg–Zn–Ca [6] and Mg–Zn–Zr [7], have been widely studied due to their high plasticity, good aging strengthening ability, and low cost [8–9]. Moreover, the mechanical properties of magnesium can be notably enhanced by adding a small amount of alloying elements to the magnesium matrix [10]. Sr and Ca as two frequently-used alloying elements were expected to exert a positive effect on overcoming the disadvantages of magnesium. Meng *et al*. [11] studied the influence mechanism of Sr addition on the microstructure of Mg–Zn–Ca alloy, and the result revealed that Sr can refine the second phases near the grain boundaries, which can effectively refine the grain sizes. Moreover, the introduction of Ca in magnesium matrix can weaken the texture [12], and the exist of Ca and Zn [13] in Mg is beneficial to activate the basal slip. Meng *et al*. [11] only added 0.3wt% Sr and 0.3wt% Ca to the magnesium matrix, and the yield strength has been greatly improved. Accordingly, a low-alloyed Mg–Zn–Sr–Ca was selected as the matrix of the composite in this work.

By adding reinforcement into magnesium matrix to prepare magnesium matrix composites is another method to optimize the mechanical properties of magnesium alloys. In our previous studies [14–15], the ultimate tensile strength (UTS) of AZ91 has been effectively increased by adding a large volume fraction micron or submicron SiC particle (SiC_p). Compared with micro reinforcement, nano-particles has a higher strengthening effect and plays a tiny influence on the ductility of magnesium matrix [16]. It is obvious that a small amount of SiC nanoparticles addition can not only enhance the yield strength (YS) of magnesium, but also retain elongation to failure (EL) [17]. Yu *et al*. [18] prepared nano-Ti particle reinforced AZ31 nanocomposites (nano-Ti_p/AZ31) by P/M (powder metallurgy) method and extrusion process. They found that the ultra-fine grain structure is obtained in the nanocomposite after extrusion and the YS of Ti_p/AZ31 increased to 341 MPa. Meenashisundaram *et al.* [19] found that 1.98vol% nano-Ti_p/Mg shows a better effect of grain reinforcement, Orowan strengthening, and dislocation strengthening. However, for nanoparticle reinforcement, whether it could effectively exert the strengthening effect is

✉ Corresponding author: Kaibo Nie E-mail: kaibo.nie@gmail.com, niekaibo@tyut.edu.cn

mainly depended on the uniform dispersion of particles [20]. Introduction of ultrasound-assisted semi-solid stirring casting method to prepare nanoparticle reinforced magnesium matrix composites [6,21] can break up the agglomeration of nanoparticles in the magnesium matrix. Moreover, hot extrusion is another method to improve the distribution of nano-reinforcement [22–23]. Qiao *et al*. [24] reported that the agglomeration of nano-SiC that existed in as-cast structure is effectively improved after extrusion deformation. The YS of nano-SiC_p/AZ91 up to 400 MPa. Among many nanoparticles, TiC nanoparticles are expected to greatly enhance the mechanical properties of magnesium alloys, which mainly benefits from their low density (4.93 g/cm^3) and superior Young's modulus (300–480 GPa) [25]. Furthermore, most of the current study focus on pure magnesium [19], magnesium alloy of AZ [14,26], and the series alloy of ZK [27]. There are also other researches focus on magnesium alloy [7,17,28] of high content of alloying element [29]. However, there are few studies on the influence of nano-TiC particles (TiC_p) on microstructure and mechanical properties of low-alloyed magnesium matrix composites. The influence of hot deformation on the microstructure and mechanical properties of nano-TiC_p reinforced low-alloyed Mg–Zn–Sr–Ca is still not clear. Thus, a kind of high strength magnesium matrix composite is hopeful to prepare by adding nano-TiC particles into Mg–Zn–Sr–Ca matrix containing low content of Zn, Sr, and Ca.

Therefore, in this paper, Mg–2Zn–0.8Sr–0.2Ca (wt%) was used as magnesium matrix, and 1.0wt% TiC_p/Mg–2Zn–0.8Sr–0.2Ca composite was successfully casted by ultrasound-assisted semi-solid stirring casting. After hot extrusion, the influence of extrusion parameters on microstructures, properties, and second phases of the composite were discussed.

2. Experimental

2.1. Preparation of nanocomposites

The matrix was Mg–2Zn–0.8Sr–0.2Ca (wt%), and the reinforcement was nano-TiC_p with an average size of 50 nm and a mass fraction of 1.0wt%, produced by Hefei Kaier Nano Energy & Technology Co. Ltd., China. First, the matrix was produced by put pure magnesium (99.98%), pure zinc (99.99%), pure calcium (99.5%), and Mg–20Sr (wt%) alloy in a stainless steel crucible heated to 750°C and protected by a mixture gas of CO_2+SF_6. Second, the semi-solid temperature interval of matrix was calculated from the Mg–Zn phase diagram and adjusted the resistance furnace temperature to 645°C. TiC_p preheated to about 200°C was added to the semi-solid alloy melt and then stirred the melt for about 15 min. After stirring, the temperature of the resistance furnace was adjusted to 720°C. Then the ultrasonic rod was put into the alloy liquid for ultrasonic dispersion treatment for about 10 min. Finally, the nanocomposite melt was poured into a mold with a temperature of 400°C and applying the 450 MPa pressure above the top of the nanocomposite melt, and then the as-cast TiC_p/Mg–Zn–Sr–Ca nanocomposite was obtained.

2.2. Extrusion of nanocomposites

The as-cast nanocomposite was cut into cylindrical specimens (ϕ40 mm × 60 mm). The specimens were solution treated at 320°C for 8 h and 430°C for 12 h. The treated sample was polished and placed in the extrusion die in the extrusion furnace to hold for 20 min. The selection of extrusion parameters were as follows: a constant extrusion ratio of 16:1, the extrusion rate of 1.0 mm/s and 0.1 mm/s under an extrusion temperature of 200°C, and extrusion temperature of 240°C under a rate of 0.1 mm/s.

2.3. Microstructure characterization of nanocomposites

Optical microscope (OM, 4 XC), scanning electron microscope (SEM, MIRA3LMH SEM), and energy spectrometer (EDS) were used to characterize the microstructure of the sample. The samples for OM and SEM were ground and etched in a mixture of 3.5wt% oxalic acid and nitric acid alcohol of 4vol% with a volume ratio of 3:2. X-ray diffraction (XRD, Rigaku SmartLab), using a Cu-K_α radiation under a rate of 2°/min over a 2θ range of 20°–80°, was used for phase analysis. Brooke D8 X-ray diffraction (XRD) was used for measuring macrotexture of the extruded samples. The size of dynamically recrystallized grains (d_{DRX}) and the volume fraction of dynamically recrystallization (V_{DRX}) were statistically analysed by Image-Pro Plus software. After that, the distribution of d_{DRX} was given by Origin.

2.4. Tensile test of nanocomposites

The mechanical properties of TiC_p/Mg–Zn–Sr–Ca nanocomposite was tested by Instron Series 3369 universal testing machine. The specimens (gauge length of 32 mm with cross-sectional area of 6 mm × 2 mm) parallel to the extrusion direction (ED) were selected for the mechanical properties test, and deformation rate was selected as 0.5mm/min. To guarantee the repeatability of results, the reported consequence of tensile properties was on the basis of the average of three tensile samples.

3. Results and discussion

3.1. Microstructure after extrusion

Fig. 1 depicts the OM images of the TiC_p/Mg–Zn–Sr–Ca nanocomposites under different extrusion parameters. It is clear that incomplete DRX occurs in the nanocomposite after extrusion by different extrusion conditions, and large deformed grains distribute along the ED. As depicted in Fig. 1(a) and (b), when extrusion temperature is 200°C under the speed of 1.0 mm/s, the V_{DRX} of the nanocomposite is 71% with the average d_{DRX} of 0.57 μm (Fig. 2(a)). As can be seen from Fig. 1(c) and (d), when the extrusion rate decreases to 0.1 mm/s, the number of large deformed grains increases, accompanied by the emergency of a large number of twins, the V_{DRX} decreases to 63%, and the grain size is significantly refined to 0.30 μm (Fig. 2(b)). When the extrusion rate remains at 0.1 mm/s but the extrusion temperature rises to 240°C, it can be found from Fig. 1(e) and (f) that the number of large deformed grains and twins decreases. Accordingly,

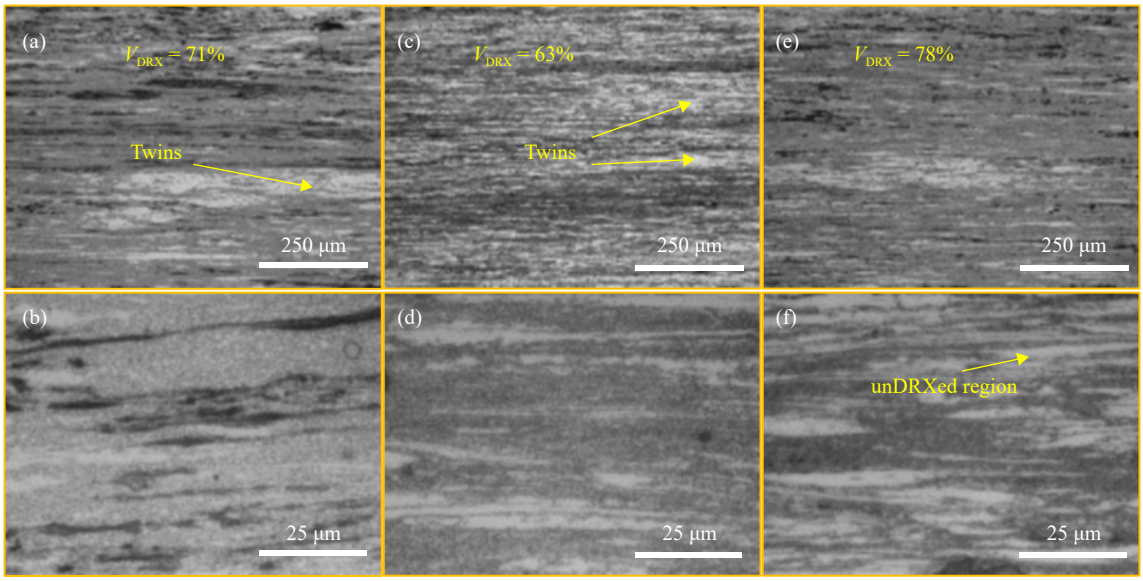

Fig. 1. OM images of the as-extruded TiC_p/Mg–Zn–Sr–Ca nanocomposites at (a, b) 200°C-1.0 mm/s, (c, d) 200°C-0.1 mm/s, and (e, f) 240°C-0.1 mm/s.

V_{DRX} increases to 78% with d_{DRX} of 0.54 μm for the sample extruded at 240°C-0.1mm/s.

As illustrated in Fig. 1(a) and (c), as the extrusion temperature remains constant, a mass of twins appears in the microstructure of as-extruded nanocomposites as the extrusion rate decreases. Generally speaking, the $\{10\bar{1}2\}$ tensile twins are more likely to be activated due to their low critical shear stress, and this type of twins will rotate 86° and distribute along the $\langle 11\bar{2}0\rangle$ direction for coordinating the deformation [30]. In addition, the factors which affected the DRXed grain size and DRX fraction mainly includes the extrusion rate and temperature. The influence of those factors on d_{DRX} can be expressed by the Zener-Hollomon parameter (Z) [31]:

$$Z = \dot{\varepsilon}\exp\left(\frac{Q}{RT}\right) \quad (1)$$

where R represents the gas constant; $\dot{\varepsilon}$ is strain rate; Q and T are activation energy and deformation temperature, respectively. Therefore, the relationship between the size of recrystallized grain and Z value can be expressed as [31]:

$$Zd_{DRX}^{m} = A \quad (2)$$

where m and A represent power law exponent and an invariable, respectively. It is obvious that the d_{DRX} decreases when Z increases according to Eq. (2). The deformation temperature reduces from 240 to 200°C and leads to the enhancement of Z. Thus, the d_{DRX} is refined which has been observed in Fig. 2(b) and (c). However, the d_{DRX} decreases by decreasing extrusion speed (Fig. 2(a) and (b)), which is inconsistent with that described by the Zener-Hollomon parameter. This is mainly because that the reduction of extrusion rate is more conducive to the emission of extrusion heat [10]. The emission of heat is not conductive to the migration of grain boundaries. Thus, the DRXed grain size is refined. When the extrusion temperature increases from 200 to 240°C under a constant extrusion speed, it can find that with the increase of extrusion temperature, the d_{DRX} and V_{DRX} of nanocomposites increases (Fig. 1(c) and (e), Fig. 2(b) and (c)). This is because the change in d_{DRX} and V_{DRX} is connected with the number of heterogeneous nucleation particles and the migration ability of grain boundaries, while the number of heterogeneous nucleation particles is related to the diffusion ability of atoms. Research [32] have shown that the increase of temperature is conducive to the diffusion of atoms. Therefore, when the extrusion temperature increases from 200 to 240°C, the diffusion of solution atoms is accelerated, so that the number of heterogeneous nucleation sites increases and V_{DRX} increases. Moreover, the migration of grain boundaries is also accelerated, leading to the increase of d_{DRX} (Fig. 2(b) and (c)).

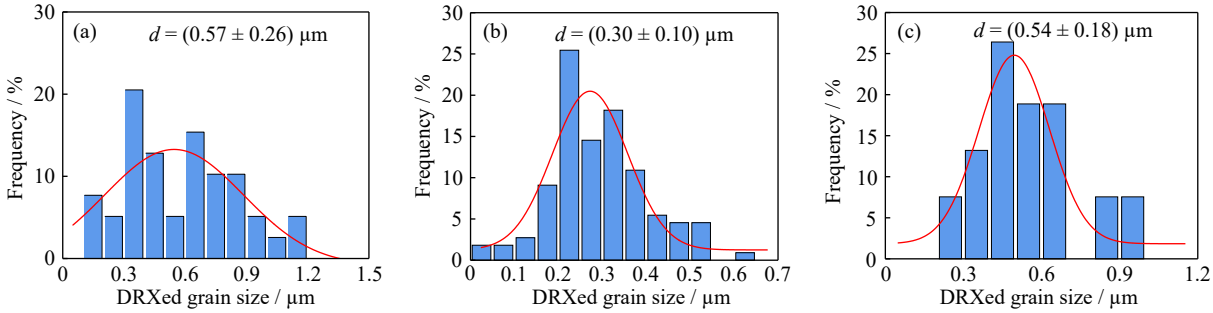

Fig. 2. Recrystallized grain size distribution of as-extruded TiC_p/Mg–Zn–Sr–Ca nanocomposites under different extrusion parameters: (a) 200°C-1.0 mm/s, (b) 200°C-0.1 mm/s, and (c) 240°C-0.1 mm/s.

Fig. 3 illustrates the secondary electron micrographs of as-extruded nanocomposite under different conditions. As depicts in Fig. 3(a), (c), and (e), it is clear that some second phases distribute along ED. There are also some broken second phases after extrusion. The number of second phases significantly increase at the extruded parameter of 200°C-0.1 mm/s. The EDS results for these second phases are shown in Table 1. From the EDS results, it is obviously that these second phases may are $MgZn_2$ phases. Further, some TiC also be detected in these positions. The XRD patterns of the extruded TiC_p/Mg–Zn–Sr–Ca nanocomposites after different extrusion parameters are demonstrated in Fig. 4. It can be further verified by XRD that the microstructure of TiC_p/Mg–Zn–Sr–Ca nanocomposite after extrusion is make up of α-Mg, TiC, and the second phases including $Ca_2Mg_6Zn_3$, $Mg_{17}Sr_2$, and $MgZn_2$.

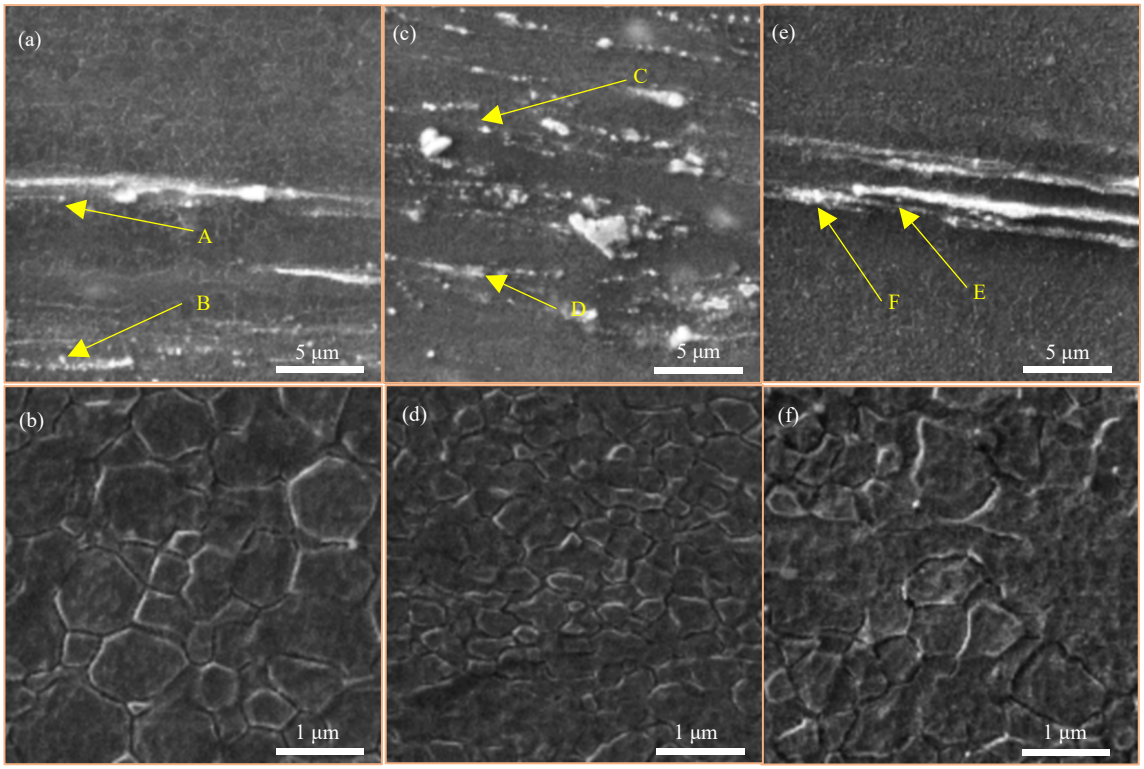

Fig. 3. SEM images of as-extruded TiC_p/Mg–Zn–Sr–Ca nanocomposites under different extrusion parameters: (a, b) 200°C-1.0 mm/s; (c, d) 200°C-0.1 mm/s; (e, f) 240°C-0.1 mm/s.

Table 1. EDS analysis of TiC_p/Mg–Zn–Sr–Ca nanocomposites for different points shown in Fig. 3

Point	Element / at%					Possible compound
	Mg	Zn	Sr	Ca	Ti	
A	92.9	1.8	0	0	5.3	$MgZn_2$, TiC
B	90.6	1.5	0	0	7.9	$MgZn_2$, TiC
C	93.1	1.9	0	0	5.0	$MgZn_2$, TiC
D	66.7	2.0	0.5	0.2	30.6	$MgZn_2$, TiC
E	92.6	1.3	0	0	6.1	$MgZn_2$, TiC
F	77.1	1.6	0.7	0.3	20.3	$MgZn_2$, TiC

3.2. Texture evolution

Fig. 5 investigates the macroscopic textures of the extruded TiC_p/Mg–Zn–Sr–Ca nanocomposites under different extrusion parameters. As the distribution of poles shown in Fig. 5, it can be concluded that all the three textures belong to $\{10\bar{1}2\}\langle 0001\rangle$ texture [33]. As depicted in Fig. 5(a), (d), and (g), the intensity of fiber texture increases, while the extrusion rate decreases from 1.0 to 0.1 mm/s. As the extrusion temperature rising from 200 to 240°C, the slight improvement on intensity of fiber texture is observed. But the fiber texture does not change significantly under three extrusion conditions. It can be noted that the texture intensity of the prismatic plane I $(10\bar{1}0)$ is significantly stronger than that of the basal plane (0002) from Fig. 5(b), (e), and (h). When the extrusion temperature is 200°C and the speed is 1.0 mm/s, the texture intensity of the prismatic plane I $(10\bar{1}0)$ of the nanocomposite reaches about 22.005 mud which is the strongest.

Generally speaking, the texture of extruded Mg matrix composites [34] is mainly affected by the DRX degree, grain size, twining, and second phases. With the change in extrusion parameters, basal texture of the material increases from 5.189 to 5.937 mud, which is mainly related to different recrystallization degree and grain size of the nanocomposite. Study has shown [35] that the basal texture intensity of the deformed structure is much higher than that of the DRXed regions, and growth of the DRXed grains can also cause the improvement of the texture intensity. With the enhancement of extrusion speed, both the V_{DRX} and the d_{DRX} of the nanocomposite (Figs. 1 and 2) increases, so the basal texture intensity decreases. When the extrusion temperature increases, both the V_{DRX} and the d_{DRX} of the nanocomposite also im-

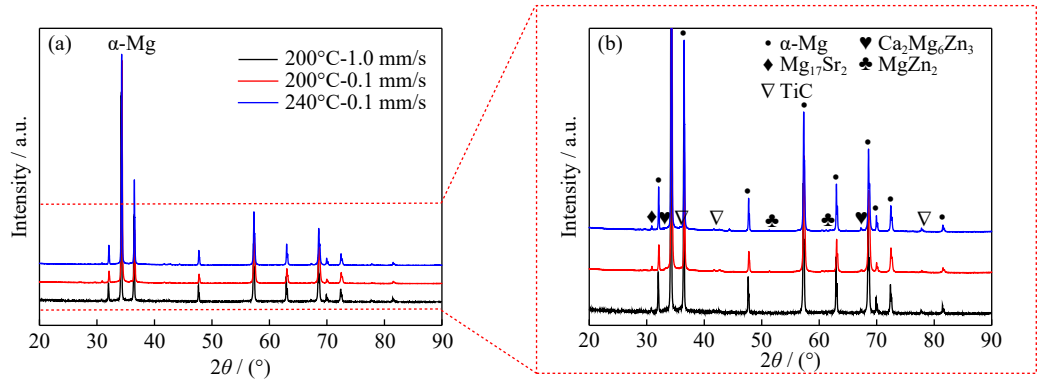

Fig. 4. (a) XRD spectra of as-extruded TiC_p/ Mg–Zn–Sr–Ca and (b) corresponding enlarged pattern as selected by red area in (a).

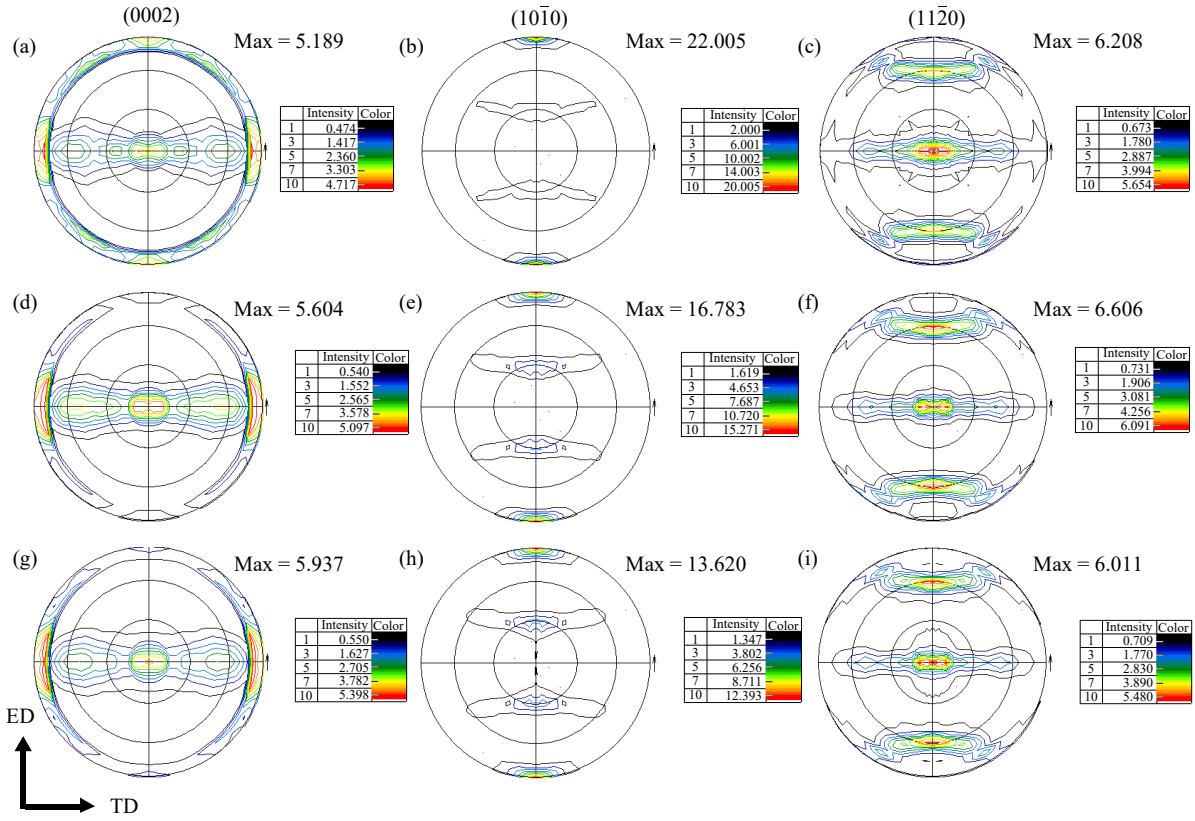

Fig. 5. (0002), (10$\bar{1}$0), and (11$\bar{2}$0) pole figures of as-extruded TiC_p/Mg–Zn–Sr–Ca nanocomposites under different extrusion parameters: (a–c) 200°C-1.0 mm/s; (d–f) 200°C-0.1 mm/s; (g–i) 240°C-0.1 mm/s.

proved. However, the change of texture intensity is converse. This is mainly due to the influence of second phases. There are more second phases at 200°C (Fig. 3) than extruded at 240°C. The second phases can inhibit dislocation slip and promote the rotation of grains, which is beneficial to weaken texture. Contrasting the prismatic I (10$\bar{1}$0) texture (Fig. 5), it shows that prismatic I texture is significantly higher than the basal texture. This is mainly due to the basal slip system is easy to activate, leading to the intensity of base plane has lower texture. As depicted in Fig. 5(b) and (e), when the extrusion temperature remains constant, the texture strength decreases with the decrease of extrusion rate. This is mainly due to with extrusion rate decrease, the d_{DRX} decreases (Fig. 2(a) and (b)), which leads to the weakening of the texture intensity of the nanocomposite. On the other hand, it is clear that twining can induce recrystallization and nucleation, and the recrystallized grains induced by twinning can randomize the texture [36], thereby weakening the strongly deformed texture. Moreover, when extruded at low rate, there are more twins exist. Thus, these two aspects together lead to weakening of the texture of the as-extruded composites at a low extrusion rate. When the extrusion rate remains at 0.1 mm/s, the DRX degree of the nanocomposite increases with the increase of extrusion temperature (Fig. 1(c) and (e)). The higher the V_{DRX} is, the more random grain orientation distribution is, the smaller texture strength is, and the material plasticity is also improved (Fig. 6(a)).

3.3. Mechanical properties

Fig. 6(a) demonstrates the engineering stress–engineering strain curves of TiC_p/Mg–Zn–Sr–Ca nanocomposites after extrusion. The UTS, YS, and EL are given in Fig. 6(b). Ta-

ble 2 depicts the comparison among the present TiC_p/Mg–Zn–Sr–Ca nanocomposites and other magnesium matrix composites. Combining with Fig. 6 and Table 2, it is obvious that the YS, UTS, and EL of the TiC_p/Mg–Zn–Sr–Ca nanocomposite is 354.8 MPa, 361.5 MPa, and 4.5%, respectively, after extrusion at 200°C-1.0 mm/s. When the extrusion rate decreases to 0.1 mm/s, the YS and UTS increases to 462.0 MPa and 480.2 MPa, respectively, while the EL decreases to 2.0%. When the extrusion rate remaining at 0.1 mm/s and the extrusion temperature increases to 240°C, the YS and UTS decreases to 418.7 MPa and 445.2 MPa, respectively. Comparing with other Mg matrix composites [6,14–15,21,26–28,37–44], the YS of the present nanocomposites are still higher than that of most other magnesium matrix (AZ91, Mg–Al–Zn, AZ31, Mg–Al–Ca, Mg–Zn–Ca, Mg–Zn–Ca–Mn, and ZK60A) composites which are reinforced by other micro or nanoscale ceramic particles. Therefore, the combination of low alloying and compounding realizes the preparation of high-strength magnesium matrix materials.

3.4. Strengthening mechanism

The dominating strengthening mechanisms for Mg matrix composites involve fine grain strengthening, Orowan strengthening and dislocation strengthening, load transfer strengthening, and thermal mismatch strengthening [38,45–46]. The added TiC_p content is 1.0wt%, so the value

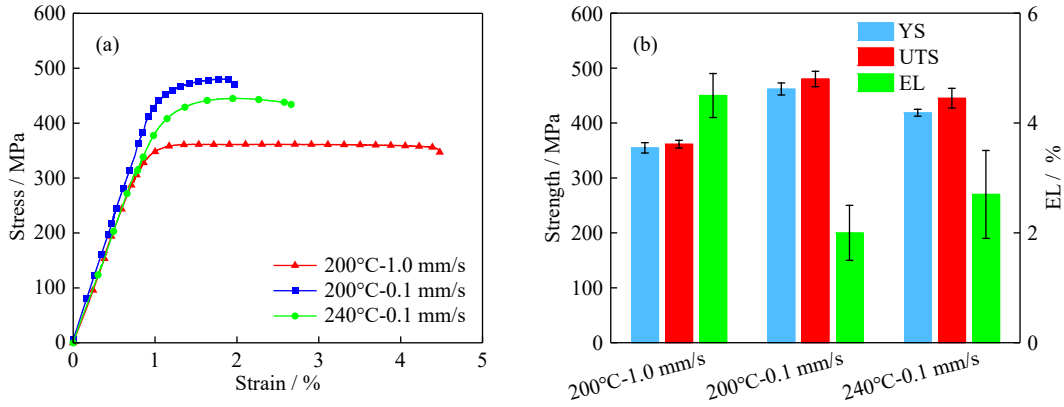

Fig. 6. (a) Tensile stress–strain curves of as-extruded TiC_p/Mg–Zn–Sr–Ca nanocomposites; (b) the YS, UTS, and EL of as-extruded TiC_p/Mg–Zn–Sr–Ca nanocomposites.

Table 2. Mechanical properties of the magnesium matrix composite reinforced by nanoparticles processed by different preparation or deformation methods

Materials	YS / MPa	UTS / MPa	EL / %
1wt% nano-TiC_p/Mg–2Zn–0.8Sr–0.2Ca (200°C-1.0 mm/s, present work)	354.8	361.5	4.5
1wt% nano-TiC_p/Mg–2Zn–0.8Sr–0.2Ca (200°C-0.1 mm/s, present work)	462.0	480.2	2.0
1wt% nano-TiC_p/Mg–2Zn–0.8Sr–0.2Ca (240°C-0.1 mm/s, present work)	418.7	445.2	2.7
5 μm SiC_p/Mg–4Zn–0.5Ca (as-extruded) [40]	322.7	409.1	10.1
0.2 μm SiC_p/AZ91 (as-extruded) [15]	275.3	335.4	2.4
S-1 + 10–9 μm SiC_p/AZ91 (as-extruded) [15]	328.8	360.1	1.28
10 μm 10vol% SiC_p/AZ91 (as-extruded) [15]	283.1	347.6	1.2
5 μm 10vol% SiC_p/Mg–Al–Zn (as-extruded) [41]	310	395	3.8
50 nm TiC_p/Mg–4Zn–0.5Ca (as-extruded) [43]	355.3	385.7	10.2
40 nm TiC_p/Mg–2.9Zn–1.1Ca–0.5Mn (as-extruded) [6]	384.5	410.3	4
1wt% nano $(SiC+TiC)_p$/AZ91 (as-extruded) [21]	345.6	397.2	5.2
5 μm SiC_p/AZ91 (as-extruded) [14]	371.5	443.9	2.5
1vol% nano-SiC_p/AZ91 (as-extruded) [39]	213	320	14.7
1vol% nano-SiC_p/AZ31 (as-extruded) [28]	225	300	8.3
2vol% nano-SiC_p/AZ31 (as-extruded) [28]	268	335	6.8
10 μm SiC_p/Mg–4Zn–0.5Ca (as-extruded) [44]	250	330	6.8
1 μm SiC_p/Mg–5Al–2Ca (as-extruded) [42]	254	307	4.5
5 μm SiC_p/Mg–5Al–2Ca (as-extruded) [42]	243	313	11
10 μm SiC_p/Mg–5Al–2Ca (as-extruded) [42]	235	300	12
30–50 nm TiC_p/Mg (as-extruded) [38]	125	190	20
50 nm TiC_p/ZK60A (as-extruded) [27]	184	309	11.6
Nano-(Al_2O_3+SiC)/Mg–3Al–1Zn (as-extruded) [26]	230	322	4.3
Nano-Al_2O_3/AZ31 (as-rolled) [37]	121	223	9

calculated by load transfer strengthening is lower than 1 MPa on the basis of our previous work [47], and the effect on the YS of nanocomposite is negligible.

The yield strength effects by grain size can be described [34,43] by the Hall–Petch relationship: $\sigma_y = \sigma_0 + kd^{-1/2}$, where σ_y represents the yield strength of composite, σ_0 expresses as the material constant, and k is the slope of Hall–Petch. The relationship for the TiC_p/Mg–Zn–Sr–Ca nanocomposite between the increasement of yield strength ($\Delta\sigma_{Hall-Petch}$) associates with the grain refinement can be described as follows [48]:

$$\Delta\sigma_{Hall-Petch} = kd^{-1/2} \tag{3}$$

where k represents the Hall–Petch coefficient of 215.6 MPa·μm$^{-1/2}$, d stands for the average grain size of the as-extruded nanocomposite. After substituting the parameters into Eq. (3), the improvement in the YS caused by $\Delta\sigma_{Hall-Petch}$ at 200°C-1.0 mm/s, 200°C-0.1 mm/s, and 240°C-0.1 mm/s can be obtained as 285.5, 393.6, and 293.4 MPa, respectively.

Moreover, the introduction of nano-TiC_p can hinder the dislocation motion and give rise to the enhancement of yield strength. In this study, the description between the increase of yield strength and Orowan strengthening can be indicated as follows [46]:

$$\Delta\sigma_{Orowan} = M\left[0.4Gb\cdot\pi^{-1}\cdot(1-\upsilon)^{-0.5}\right]\cdot \left[(4f-1)^{0.5}\cdot\pi^{-0.5}\right]\cdot\bar{d}^{-1}\ln(\bar{d}/b) \tag{4}$$

where M is the strengthening coefficient (1.25); G, b, and υ are the shear modulus of matrix (16.6 GPa), Burger's vector (0.32 nm), and Poisson's ratio (0.35), respectively; $\bar{d} = \sqrt{\frac{2}{3}}d_p$; f and d represent the particle volume fraction and average size, respectively. Therefore, the enhancement in the YS contributed by $\Delta\sigma_{Orowan}$ is 53.8 MPa according to Eq. (4).

In wrought magnesium alloys, the dislocation density has a huge difference between the DRX region and the unDRX region. The formation of DRX grains is a process that consumes dislocations. Therefore, the dislocation density in the DRX region is much smaller than that in the unDRX region. In addition, the dislocation density is generally difficult to determine. The main contribution of dislocation strengthening comes from the unDRX region. Study has shown [49] that the dislocation density in the unDRX region of metal material with a large amount of deformation is about 10^{15}–10^{16} m^{-2}, so the dislocation density of 10^{16} m^{-2} is selected in this work. Dislocation strengthening contributing to the increase in yield strength can be expressed by the following formula:

$$\Delta\sigma_{Dislocation} = f_{unDRX}\cdot M\alpha Gb\sqrt{\rho} \tag{5}$$

where f_{unDRX} is the unDRX volume fraction of the composite material; α is a constant (0.2); ρ stands for the dislocation density. Thus, the corresponding value of $\Delta\sigma_{Dislocation}$ under 200°C-1.0 mm/s, 200°C-0.1 mm/s, and 240°C-0.1 mm/s extrusion are 37, 47.1, and 28.1 MPa, respectively.

In addition, the different thermal expansion coefficients between TiC_p and magnesium matrix can also cause the increase in YS, which can be expressed as follows [50]:

$$\Delta\sigma_{CTE} = \sqrt{3}MGb\sqrt{\frac{12\Delta\alpha\Delta T f}{bd_p}} \tag{6}$$

where $\Delta\sigma_{CTE}$ is the yield strength of the nanocomposites caused by thermal mismatch. $\Delta\alpha$ and ΔT respectively stands for the difference of thermal expansion coefficient between TiC nanoparticles (7.4 × 10^{-6} K^{-1}) and magnesium matrix (30.7 × 10^{-6} K^{-1}) and the temperature gradient on the mechanical measure and hot deformation. Therefore, at 200°C and 240°C, the increasement of yield strength caused by thermal mismatch is 37.2 and 69.06 MPa, respectively.

Therefore, the theoretical yield strength (σ_y) of TiC_p/Mg–Zn–Sr–Ca nanocomposite can be indicated by the modified Clyne model with the equation as [46]:

$$\sigma_y = \sigma_{matrix} + \sqrt{\Delta\sigma^2_{Hall-Petch} + \Delta\sigma^2_{Orowan} + \Delta\sigma^2_{Dislocation} + \Delta\sigma^2_{CTE}} \tag{7}$$

where σ_{matrix} is the material constant, which can be deemed as 61 MPa on the basis of the yield strength of the as-cast nanocomposite [51]. Fig. 7(b) illustrates the comparison between the theoretical value and the experimental value of the yield strength based on as-extruded nanocomposite. It can be found that the nanocomposite extrudes at 200°C, the theoretical YS value is in good agreement with the tested YS value, and the grain refinement plays a crucial role in the YS increasement (Fig. 7(a)). When the nanocomposite extrudes at 240°C, the theoretically calculated YS value is inferior to the tested YS value. This is mainly due to the fact that more fine phases precipitate near the grain boundaries (Fig. 3(g)). The finely dispersed second phases can hinder the movement of dislocations, which causing an increasement in the yield strength. The contribution of these precipitates to the yield strength is difficult to calculate accurately, and the contribution of this part is ignored, which ultimately resulting in theoretical YS value lower than tested YS value.

Fig. 8(a)–(c) illustrates the OM images near the fracture surface of TiC_p/Mg–Zn–Sr–Ca nanocomposites extruded under different conditions. There are twins included in unDRX region in both as-extruded nanocomposites which can be confirmed by Fig. 8(a)–(c). As illustrated in Fig. 8(a) and (b), when extrusion temperature maintains at 200°C and extrusion rate decreases, the unDRX area increases, and there exists a mass of twins in the unDRX area. In addition, banded structures are also found in the microstructure. The coarse second phases are included in these banded structure (Fig. 3). Thus, these banded structures are easy to be the source of cracks. And the number of banded structure increases with the decrease of extrusion rate, which leads to a loss in the elongation of the nanocomposites. As shown in Fig. 8(b) and (c), when the extrusion rate remains at 0.1 mm/s and the extrusion temperature increases to 240°C, it can be found that the unDRX region, the number of twins, and the number of banded structure all decreases, thus its elongation increases (Fig. 6).

Fig. 9(a), (c), and (e) shows the SEM morphology of the fracture of TiC_p/Mg–Zn–Sr–Ca nanocomposite extruded un-

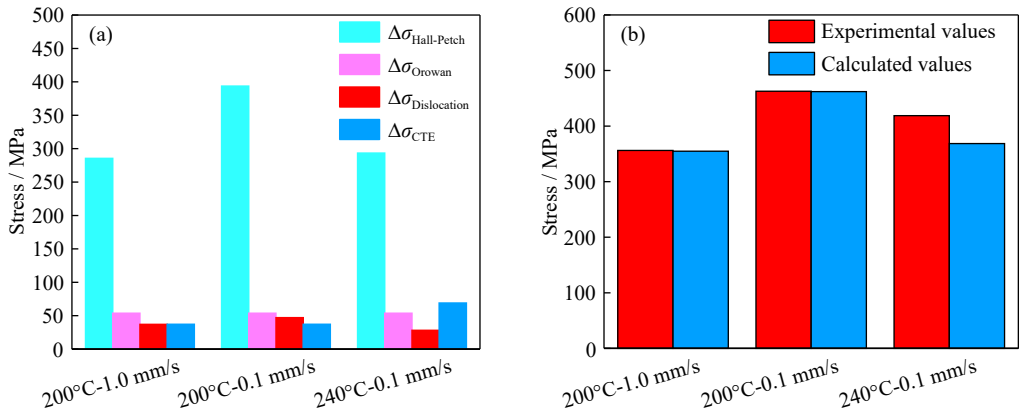

Fig. 7. (a) Contributions of various strengthening mechanisms of as-extruded 1.0wt%TiC_p/Mg–2Zn–0.8Sr–0.2Ca nanocomposite; (b) comparison of the theoretical value and the experimental value of the yield strength.

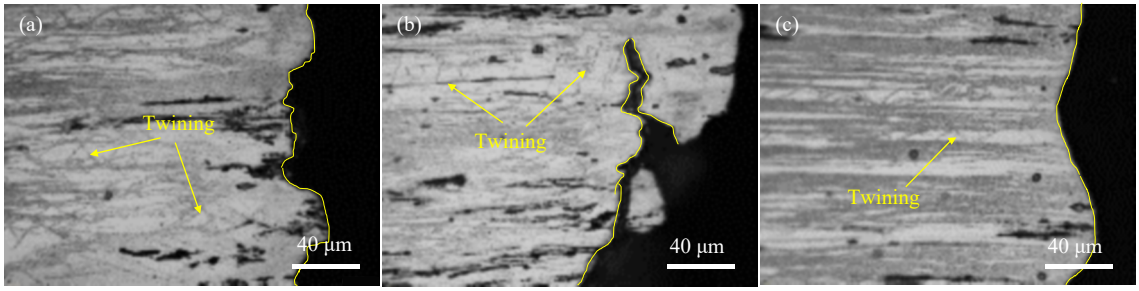

Fig. 8. OM images of side fracture of as-extruded TiC_p/Mg–Zn–Sr–Ca nanocomposites: (a) 200°C-1.0 mm/s; (b) 200°C-0.1 mm/s; (c) 240°C-0.1 mm/s.

der different parameters. Fig. 9(b), (d), and (f) is the corresponding SEM images at high magnification. Compared with Fig. 9(a) and (c), it can be clearly noted when the temperature remains at 200°C and the extrusion speed decreases, the fracture presents an obviously large cleavage surface, which is a typical morphology of brittle fracture. However, when the speed increases to 1.0 mm/s, there are a lot of dimples in the fracture surface. Therefore, the plasticity of material de-

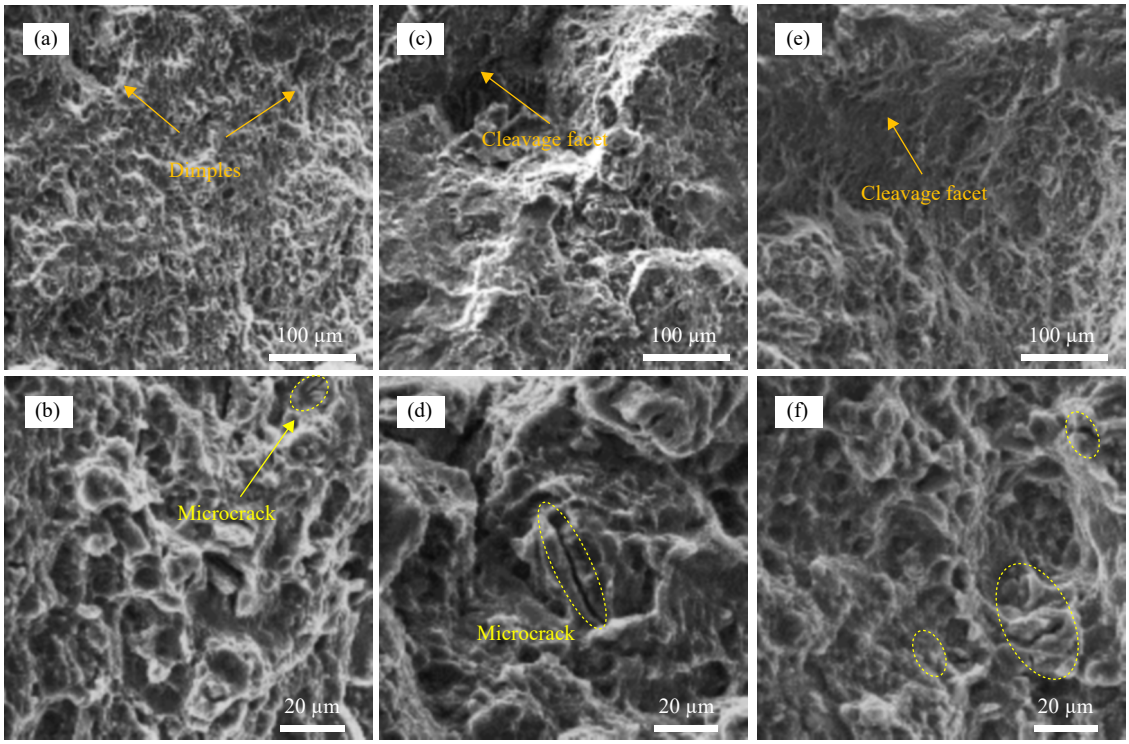

Fig. 9. SEM fracture surface morphologies of as-extruded TiC_p/Mg–Zn–Sr–Ca nanocomposites: (a, b) 200°C-1.0 mm/s; (c, d)200°C-0.1 mm/s; (e, f) 240°C-0.1 mm/s.

creases after decreasing the extrusion rate. As observed from Fig. 9(c) and (e), at the same extrusion rate of 0.1mm/s, when the extrusion temperature increases from 200 to 240°C, there still exists cleavage surface in the fracture. But the number of dimples in the fracture increases, which is mainly due to the enhancement of DRX volume fraction caused by the increasement of extrusion temperature. At the same time, the massive microcrack disappears, which can be reflected in Fig. 9(d) and (f). Therefore, the EL increases.

4. Conclusions

In this study, the microstructure and tensile properties of TiC_p/Mg–2Zn–0.8Sr–0.2Ca (wt%) nanocomposite extruded at different temperatures and rates are investigated, and the dominating conclusions are concluded as follows.

(1) With the decrease of extrusion rate, both the recrystallization rate and recrystallized grain size of nanocomposite decreases, and the recrystallization rate arises with the increase of extrusion temperature. The finest grain size (~0.30 μm) were obtained under 200°C-0.1 mm/s.

(2) The ultra-high properties of the material (UTS of 480 MPa, YS of 462 MPa) were obtained after extrusion at 200°C-0.1 mm/s. The high strength mainly results from grain refinement strengthening, Orowan strengthening, dislocation strengthening, load transfer strengthening, and thermal mismatch strengthening.

(3) With the change of extrusion parameters, the prismatic texture of the nanocomposite has a significant change, which are mainly influenced by grain size and the DRX degree. The strongest prismatic texture (22.005 mud) appeared under extrusion at 200°C-1.0 mm/s.

(4) The banded structures in the nanocomposites are easy to be the origination of the crack source, and a mixture of cleavage facets and dimples were observed in fracture surface, which is a brittle-ductile fracture mechanism.

Acknowledgements

This work was financially supported by the National Natural Science Foundation of China (Nos. 51771129, 51401144, and 51771128); the Program for the Outstanding Innovative Teams of Higher Learning Institutions of Shanxi, China; the Natural Science Foundation of Shanxi Province, China (Nos. 2015021067 and 201601D011034); the Projects of International Cooperation in Shanxi, China (No. 2017 03D421039).

Conflict of Interest

The authors declare no conflict of interest.

References

[1] J.F. Song, J. She, D.L. Chen, and F.S. Pan, Latest research advances on magnesium and magnesium alloys worldwide, *J. Magnes. Alloys*, 8(2020), No. 1, p. 1.

[2] H.C. Pan, R. Kang, J.R. Li, H.B. Xie, Z.R. Zeng, Q.Y. Huang, C.L. Yang, Y.P. Ren, and G.W. Qin, Mechanistic investigation of a low-alloy Mg–Ca-based extrusion alloy with high strength–ductility synergy, *Acta Mater.*, 186(2020), p. 278.

[3] X.J. Wang, D.K. Xu, R.Z. Wu, X.B. Chen, Q.M. Peng, L. Jin, Y.C. Xin, Z.Q. Zhang, Y. Liu, X.H. Chen, G. Chen, K.K. Deng, and H.Y. Wang, What is going on in magnesium alloys?, *J. Mater. Sci. Technol.*, 34(2018), No. 2, p. 245.

[4] G.Z. Kang and H. Li, Review on cyclic plasticity of magnesium alloys: Experiments and constitutive models, *Int. J. Miner. Metall. Mater.*, 28(2021), No. 4, p. 567.

[5] M. Shahin, K. Munir, C.E. Wen, and Y.C. Li, Magnesium matrix nanocomposites for orthopedic applications: A review from mechanical, corrosion, and biological perspectives, *Acta Biomater.*, 96(2019), p. 1.

[6] K.B. Nie, Z.H. Zhu, P. Munroe, K.K. Deng, and J.G. Han, Effect of extrusion speed on mixed grain microstructure and tensile properties of a Mg–2.9Zn–1.1Ca–0.5Mn nanocomposite reinforced by a low mass fraction of TiCp, *Mater. Sci. Eng. A*, 796(2020), art. No. 140223.

[7] H.Y. Jeong, B. Kim, S.G. Kim, H.J. Kim, and S.S. Park, Effect of Ce addition on the microstructure and tensile properties of extruded Mg–Zn–Zr alloys, *Mater. Sci. Eng. A*, 612(2014), p. 217.

[8] C.J. Bettles, M.A. Gibson, and K. Venkatesan, Enhanced age-hardening behaviour in Mg–4 wt.% Zn micro-alloyed with Ca, *Scripta Mater.*, 51(2004), No. 3, p. 193.

[9] R. Alizadeh, J.Y. Wang, and J. LLorca, Precipitate strengthening of pyramidal slip in Mg–Zn alloys, *Mater. Sci. Eng. A*, 804(2021), art. No. 140697.

[10] T. Nakata, T. Mezaki, R. Ajima, C. Xu, K. Oh-Ishi, K. Shimizu, S. Hanaki, T.T. Sasaki, K. Hono, and S. Kamado, High-speed extrusion of heat-treatable Mg–Al–Ca–Mn dilute alloy, *Scripta Mater.*, 101(2015), p. 28.

[11] X. Meng, Z.T. Jiang, S.J. Zhu, and S.K. Guan, Effects of Sr addition on microstructure, mechanical and corrosion properties of biodegradable Mg–Zn–Ca alloy, *J. Alloys Compd.*, 838(2020), art. No. 155611.

[12] J.Y. Wang, Y.W. Chen, Z. Chen, J. Llorca, and X.Q. Zeng, Deformation mechanisms of Mg–Ca–Zn alloys studied by means of micropillar compression tests, *Acta Mater.*, 217(2021), art. No. 117151.

[13] Y. Liu, N. Li, M. Arul Kumar, S. Pathak, J. Wang, R.J. McCabe, N.A. Mara, and C.N. Tomé, Experimentally quantifying critical stresses associated with basal slip and twinning in magnesium using micropillars, *Acta Mater.*, 135(2017), p. 411.

[14] X.F. Sun, C.J. Wang, K.K. Deng, K.B. Nie, X.C. Zhang, and X.Y. Xiao, High strength SiCp/AZ91 composite assisted by dynamic precipitated $Mg_{17}Al_{12}$ phase, *J. Alloys Compd.*, 732(2018), p. 328.

[15] K.K. Deng, J.Y. Shi, C.J. Wang, X.J. Wang, Y.W. Wu, K.B. Nie, and K. Wu, Microstructure and strengthening mechanism of bimodal size particle reinforced magnesium matrix composite, *Compos. A: Appl. Sci. Manuf.*, 43(2012), No. 8, p. 1280.

[16] K.B. Nie, X.J. Wang, K.K. Deng, X.S. Hu, and K. Wu, Magnesium matrix composite reinforced by nanoparticles – A review, *J. Magnes. Alloys*, 9(2021), No. 1, p. 57.

[17] C.P. Li, Z.G. Wang, H.Y. Wang, X. Zhu, M. Wu, and Q.C. Jiang, Fabrication of nano-SiC particulate reinforced Mg–8Al–1Sn composites by powder metallurgy combined with hot extrusion, *J. Mater. Eng. Perform.*, 25(2016), No. 11, p. 5049.

[18] H. Yu, H.P. Zhou, Y. Sun, L.L. Ren, Z.P. Wan, and L.X. Hu, Microstructures and mechanical properties of ultrafine-grained Ti/AZ31 magnesium matrix composite prepared by powder metallurgy, *Adv. Powder Technol.*, 29(2018), No. 12, p. 3241.

[19] G.K. Meenashisundaram and M. Gupta, Low volume fraction

nano-titanium particulates for improving the mechanical response of pure magnesium, *J. Alloys Compd.*, 593(2014), p. 176.
[20] X.J. Wang, K. Wu, H.F. Zhang, W.X. Huang, H. Chang, W.M. Gan, M.Y. Zheng, and D.L. Peng, Effect of hot extrusion on the microstructure of a particulate reinforced magnesium matrix composite, *Mater. Sci. Eng. A*, 465(2007), No. 1-2, p. 78.
[21] Y.C. Guo, K.B. Nie, X.K. Kang, K.K. Deng, J.G. Han, and Z.H. Zhu, Achieving high-strength magnesium matrix nanocomposite through synergistical effect of external hybrid (SiC+TiC) nanoparticles and dynamic precipitated phase, *J. Alloys Compd.*, 771(2019), p. 847.
[22] F. Samadpour, G. Faraji, and A. Siahsarani, Processing of AM60 magnesium alloy by hydrostatic cyclic expansion extrusion at elevated temperature as a new severe plastic deformation method, *Int. J. Miner. Metall. Mater.*, 27(2020), No. 5, p. 669.
[23] Z. Zhang, J.H. Zhang, J. Wang, Z.H. Li, J.S. Xie, S.J. Liu, K. Guan, and R.Z. Wu, Toward the development of Mg alloys with simultaneously improved strength and ductility by refining grain size via the deformation process, *Int. J. Miner. Metall. Mater.*, 28(2021), No. 1, p. 30.
[24] X.G. Qiao, T. Ying, M.Y. Zheng, E.D. Wei, K. Wu, X.S. Hu, W.M. Gan, H.G. Brokmeier, and I.S. Golovin, Microstructure evolution and mechanical properties of nano-SiCp/AZ91 composite processed by extrusion and equal channel angular pressing (ECAP), *Mater. Charact.*, 121(2016), p. 222.
[25] X.Y. Tao, J. Du, Y.C. Yang, Y.P. Li, Y. Xia, Y.P. Gan, H. Huang, W.K. Zhang, and X.D. Li, TiC nanorods derived from cotton fibers: Chloride-assisted VLS growth, structure, and mechanical properties, *Cryst. Growth Des.*, 11(2011), No. 10, p. 4422.
[26] M.J. Shen, W.F. Ying, X.J. Wang, M.F. Zhang, and K. Wu, Development of high performance magnesium matrix nanocomposites using nano-SiC particulates as reinforcement, *J. Mater. Eng. Perform.*, 24(2015), No. 10, p. 3798.
[27] M. Paramsothy, J. Chan, R. Kwok, and M. Gupta, Adding TiC nanoparticles to magnesium alloy ZK60A for strength/ductility enhancement, *J. Nanomater.*, 2011(2011), art. No. 642980.
[28] M. Rashad, F.S. Pan, W. Guo, H. Lin, M. Asif, and M. Irfan, Effect of alumina and silicon carbide hybrid reinforcements on tensile, compressive and microhardness behavior of Mg–3Al–1Zn alloy, *Mater. Charact.*, 106(2015), p. 382.
[29] S.S. Shuai, E.Y. Guo, J. Wang, A.B. Phillion, T. Jing, Z.M. Ren, and P.D. Lee, Synchrotron tomographic quantification of the influence of Zn concentration on dendritic growth in Mg–Zn alloys, *Acta Mater.*, 156(2018), p. 287.
[30] K.B. Nie, Z.H. Zhu, P. Munroe, K.K. Deng, and J.G. Han, The effect of Zn/Ca ratio on the microstructure, texture and mechanical properties of dilute Mg–Zn–Ca–Mn alloys that exhibit superior strength, *J. Mater. Sci.*, 55(2020), No. 8, p. 3588.
[31] K.B. Nie, Z.H. Zhu, P. Munroe, K.K. Deng, and J.G. Han, Microstructure, tensile properties and work hardening behavior of an extruded Mg–Zn–Ca–Mn magnesium alloy, *Acta Metall. Sin. Engl. Lett.*, 33(2020), No. 7, p. 922.
[32] B.C. Zhou, S.L. Shang, Y. Wang, and Z.K. Liu, Diffusion coefficients of alloying elements in dilute Mg alloys: A comprehensive first-principles study, *Acta Mater.*, 103(2016), p. 573.
[33] Y.N. Wang and J.C. Huang, Texture analysis in hexagonal materials, *Mater. Chem. Phys.*, 81(2003), No. 1, p. 11.
[34] A. Yang, K.B. Nie, K.K. Deng, and Y.N. Li, Improved tensile properties of low-temperature and low-speed extruded Mg–χAl–(4.8−χ)Ca–0.6Mn alloys, *J. Mater. Res. Technol.*, 9(2020), No. 5, p. 11717.
[35] Y.Z. Du, X.G. Qiao, M.Y. Zheng, K. Wu, and S.W. Xu, Development of high-strength, low-cost wrought Mg–2.5 mass% Zn alloy through micro-alloying with Ca and La, *Mater. Des.*, 85(2015), p. 549.
[36] D.K. Guan, W.M. Rainforth, L. Ma, B. Wynne, and J.H. Gao, Twin recrystallization mechanisms and exceptional contribution to texture evolution during annealing in a magnesium alloy, *Acta Mater.*, 126(2017), p. 132.
[37] M. Habibnejad-Korayem, R. Mahmudi, and W.J. Poole, Work hardening behavior of Mg-based nano-composites strengthened by Al_2O_3 nano-particles, *Mater. Sci. Eng. A*, 567(2013), p. 89.
[38] G.K. Meenashisundaram and M. Gupta, Synthesis and characterization of high performance low volume fraction TiC reinforced Mg nanocomposites targeting biocompatible/structural applications, *Mater. Sci. Eng. A*, 627(2015), p. 306.
[39] K.B. Nie, X.J. Wang, K. Wu, L. Xu, M.Y. Zheng, and X.S. Hu, Processing, microstructure and mechanical properties of magnesium matrix nanocomposites fabricated by semisolid stirring assisted ultrasonic vibration, *J. Alloys Compd.*, 509(2011), No. 35, p. 8664.
[40] W.J. Li, K.K. Deng, X. Zhang, C.J. Wang, J.W. Kang, K.B. Nie, and W. Liang, Microstructures, tensile properties and work hardening behavior of SiCp/Mg–Zn–Ca composites, *J. Alloys Compd.*, 695(2017), p. 2215.
[41] S.J. Shang, K.K. Deng, K.B. Nie, J.C. Li, S.S. Zhou, F.J. Xu, and J.F. Fan, Microstructure and mechanical properties of SiCp/Mg–Al–Zn composites containing $Mg_{17}Al_{12}$ phases processed by low-speed extrusion, *Mater. Sci. Eng. A*, 610(2014), p. 243.
[42] X. Zhang, K.K. Deng, W.J. Li, H.X. Wang, K.B. Nie, F.J. Xu, and W. Liang, Microstructure and mechanical properties of Mg–Al–Ca alloy influenced by SiCp size, *Mater. Sci. Eng. A*, 647(2015), p. 15.
[43] K.B. Nie, Y.C. Guo, K.K. Deng, and X.K. Kang, High strength TiCp/Mg–Zn–Ca magnesium matrix nanocomposites with improved formability at low temperature, *J. Alloys Compd.*, 792(2019), p. 267.
[44] X.J. Wang, K.B. Nie, X.S. Hu, Y.Q. Wang, X.J. Sa, and K. Wu, Effect of extrusion temperatures on microstructure and mechanical properties of SiCp/Mg–Zn–Ca composite, *J. Alloys Compd.*, 532(2012), p. 78.
[45] J.W. Kang, X.F. Sun, K.K. Deng, F.J. Xu, X. Zhang, and Y. Bai, High strength Mg–9Al serial alloy processed by slow extrusion, *Mater. Sci. Eng. A*, 697(2017), p. 211.
[46] A. Sanaty-Zadeh, Comparison between current models for the strength of particulate-reinforced metal matrix nanocomposites with emphasis on consideration of Hall–Petch effect, *Mater. Sci. Eng. A*, 531(2012), p. 112.
[47] K.B. Nie, K.K. Deng, X.J. Wang, T. Wang, and K. Wu, Influence of SiC nanoparticles addition on the microstructural evolution and mechanical properties of AZ91 alloy during isothermal multidirectional forging, *Mater. Charact.*, 124(2017), p. 14.
[48] K.B. Nie, Z.H. Zhu, K.K. Deng, and J.G. Han, Effect of extrusion temperature on microstructure and mechanical properties of a low-alloying and ultra-high strength Mg–Zn–Ca–Mn matrix composite containing trace TiC nanoparticles, *J. Magnes. Alloys*, 8(2020), No. 3, p. 676.
[49] Y.Z. Du, X.G. Qiao, M.Y. Zheng, K. Wu, and S.W. Xu, The microstructure, texture and mechanical properties of extruded Mg–5.3Zn–0.2Ca–0.5Ce (wt%) alloy, *Mater. Sci. Eng. A*, 620(2015), p. 164.
[50] M. Habibnejad-Korayem, R. Mahmudi, and W.J. Poole, Enhanced properties of Mg-based nano-composites reinforced with Al_2O_3 nano-particles, *Mater. Sci. Eng. A*, 519(2009), No. 1-2, p. 198.
[51] K.B. Nie, J.G. Han, K.K. Deng, and Z.H. Zhu, Simultaneous improvements in tensile strength and elongation of a Mg–2Zn–0.8Sr–0.2Ca alloy by a combination of microalloying and low content of TiC nanoparticles, *Mater. Lett.*, 260(2020), art. No. 126951.